Journal of Engineering and Applied Science Vol. 07, No. 01, pp. 80–86, December 2023

Journal of Engineering and Applied Science

Contents are available at www.jeas.ruet.ac.bd

Design and Modelling of a Coaxial Probe Fed Two-Port Dual-Band Antenna for Wireless Communication

Md. Masud Rana[1], Md. Ariful Islam[2]

[1,2]*Electrical & Electronic Engineering, Rajshahi University of Engineering & Technology, Bangladesh*

ARTICLE INFORMATION

Received date: 12th Oct 2023
Revised date: 22st Dec 2023
Accepted date: 31st Dec 2023

Keywords

Wireless Communication
Dual-Band
Patch Slots
Shortening Pin
Coaxial Probe Feeding

ABSTRACT

This paper presents a dual-band antenna with coaxial probe feeding for wireless applications. The antenna consists of two spiral patches, resulting in a compact size of 27 × 14 × 1.6 mm^3. Utilizing two spiral patch elements, the antenna can operate in two frequency bands, 241-641 MHz and 1.33-2.01 GHz, providing coverage for the medical implant communication service (MICS) band and the long (L) band. As a result, it comprises the versatility to be employed in biomedical applications as well as in mobile or satellite communications. This design offers improved return loss and higher bandwidths that are achieved by incorporating patch slots and shortening pins, representing a significant contribution to the field of wireless communication. The obtained return losses are -31.98 dB and -33.16 dB at the resonant frequencies of 459 MHz and 1.68 GHz, respectively. The gain values at these resonant frequencies are -45.6 dB and -18.2 dB.

1. Introduction

In the new era of the Internet of Things (IoT), smart devices around us are now wirelessly connected [1]. Wireless Body Area Networks (WBANs), Wireless Local Area Network (WLAN) and Worldwide Interoperability for Microwave Access (WiMAX) are becoming crucial to the integration of the IoT ecosystem [1]. In the literature, numerous approaches exist for developing antennas for wireless systems. Among them is the use of slots in radiators [2], spiral patches [3], circular patches [4], defective ground structure (DGS) [5], and fractal structure [6]. A differentially fed dual-band antenna can be used for a fully implantable neuro-microsystem [7]. It enables sub-GHz wideband transmission, allowing high-data-rate implanted brain recording devices to operate. Later, spiral and serpentine shaped antennas are also utilized for operating in the MICS band [8]. Important antenna parameters can be evaluated using the finite difference time domain (FDTD) method, and results can be compared to measurements. Wireless biotelemetry systems can also use antennas based on radio frequency identification (RFID) [9]. A planar inverted-F antenna (PIFA) structured antenna can serve wireless applications. For example, a PIFA structured antenna is developed for triple-band applications, as described in [10]. The model of this antenna has four layers. Layer 1 of the antenna serves as the ground plane, whereas layers 2, 3, and 4 contain the radiating components. Wireless applications can make use of ultra-miniaturized patch antennas fed by coplanar waveguides (CPW) and ground plane slots [11]. With the use of an umbrella-shaped metallic ground

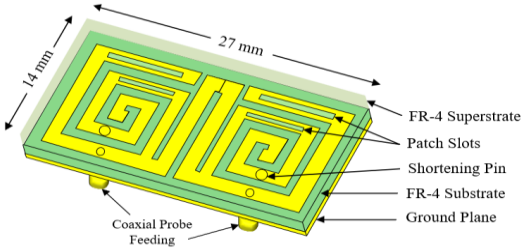

Figure 1. Proposed antenna geometry.

* Corresponding authors: Electrical & Electronic Engineering, Rajshahi University of Engineering & Technology, Bangladesh
E-mail addresses: md.masud.rana@eee.ruet.ac.bd (Md. Masud Rana)

Table 1. Optimized parameters of the proposed antenna.

Parameter	Value (mm)	Parameter	Value (mm)
l	13.5	i	0.4
b	14.0	j	0.5
c	1.5	k	0.3
d	0.8	m	1.6
f	1.0	n	0.035
g	0.5	p	4.8
h	0.9		

plane (UsMGP) and an improved radiator, a compact broadband and radiation efficient antenna can be developed [12]. An antenna with the integration of DGS and electromagnetic band-gap (EBG) with symmetrical e-slot is explained in [13]. The function of DGS is to increase the bandwidth, while EBG isolates the body and antenna from each other. A wideband ultra-compact implanted antenna (WUCIA) is proposed in [14].

The WUCIA was made up of a partial ground and a meandering radiator patch with variously shaped slots. The ultra-compact dimensions, low power loss, and compliance with safety standards. In [15], an antenna based on a stacked PIFA structure is presented, with a slot placed in each radiating patch. Again, a L-shaped transmission line fed anti-spiral resonator structure can be used for dual-band operation [16]. Dual-band coverage, higher return loss, and higher electrical length are the most advantageous characteristics of such antennas. Ultrawideband antennas with stable impedance matching are used to mitigate detuning effects for multiple wireless applications. Such antennas can be designed with two-sectioned spiral-shaped radiating patch and a slotted ground [17].

Most of the described antennas feature complex structures that are either too complicated to manufacture or too complex for modern wireless devices. Though the reported structures achieve the threshold values of the antenna parameters, these parameters can still be improved.

In this paper, we propose an antenna design that effectively operates in two separate bands. One is the MICS band, which is used in biomedical applications;

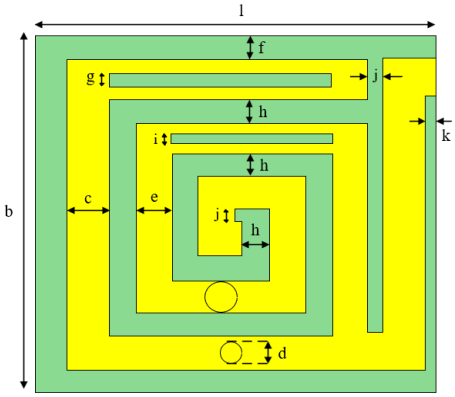

(a)

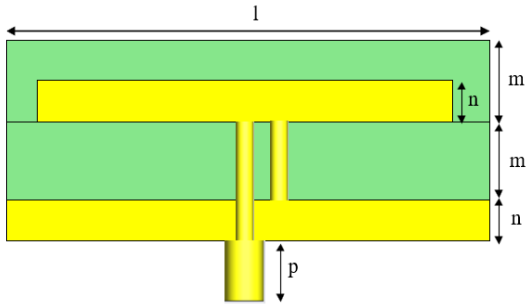

(b)

Figure 2. (a) Front view, and (b) side view of a single element.

other one is L band mobile and satellite communication in non-line of sight (NLOS) conditions. The antenna design is based on merging two spiral patch antennas together and feeding each patch individually. Patch slots are used to improve return losses and increase bandwidths. Also, shortening pins are used to tune the resonant frequencies.

2. Antenna Design Methodology

2.1. Geometry of the Proposed Antenna

Figure 1 shows the geometry of the designed antenna. It comprises two spiral components. They are connected through a spiral shaped branch which results in two frequency bands. The nearness of the patches creates electromagnetic coupling, which interacts with their individual resonances. This interaction leads to two separate frequency bands depending on the coupling strength and configuration. Both of the antenna elements are 13.5 × 14 mm^2 in size. They are symmetrically aligned, having a total size of 27 × 14 mm^2. The coaxial probe feeding technique is used to feed each antenna element. The key benefit of this feeding technique is the flexibility with which the feed can be positioned on the patch to match the cable impedance to the antenna input impedance. The suggested antenna model allows dual-band operation in the MICS band and the L band. The developed antenna is developed on a 1.6 mm FR-4 substrate. A parametric investigation is conducted to evaluate its performance and determine its optimal parameters.

The suggested antenna model allows dual-band operation in the MICS band and the L band. The developed antenna is developed on a 1.6 mm FR-4 substrate. A parametric investigation is conducted to evaluate its performance and determine its optimal parameters.

Patch slots and shortening pins are incorporated into the proposed antenna. Patch slots are used to improve return losses and increase bandwidths. Additionally, the

resonant frequencies are adjusted using a shortening pin. Single element of the proposed antenna is presented with the dimensions of the parameters in Figure 2. The optimized values of the parameters of the proposed antenna are mentioned in Table 1.

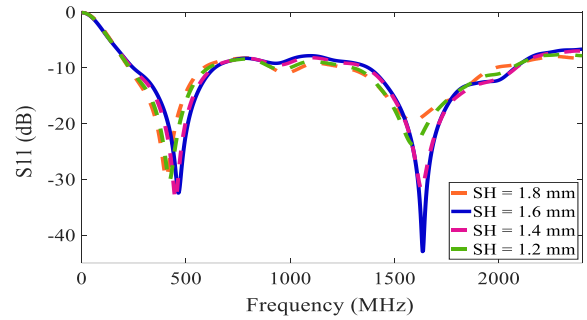

(a)

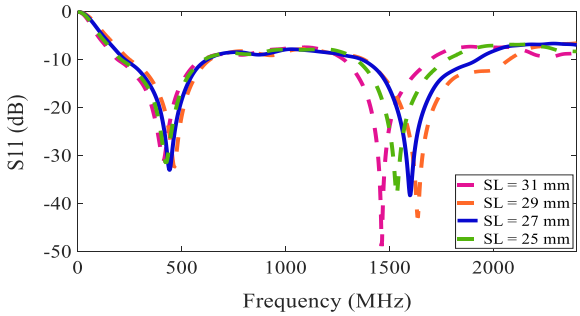

(b)

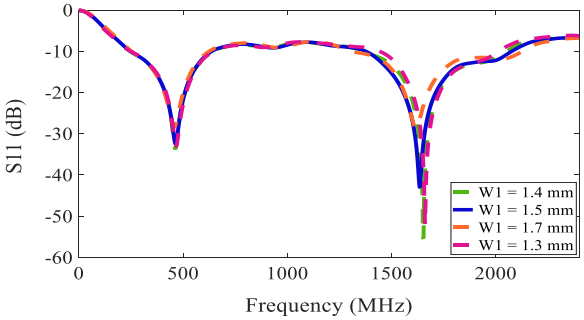

(c)

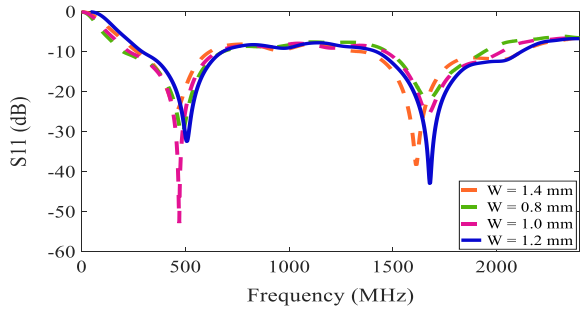

(d)

Figure 3. The effects of (a) substrate height (SH), (b) substrate length (SL), outer spiral patch width (W1), and inner spiral patch width (W) on the return loss S11 of the proposed antenna.

2.2 Investigation

Effects of several dimensional parameters on resonant frequencies, bandwidth, and impedance matching properties are analyzed through a detailed parametric investigation.

Substrate height, substrate length, substrate material, spiral arm width, patch slots, etc., are the factors that influence the antenna performance parameters.

The simulated S_{11} with varied values of substrate height (SH) is shown in Figure 3 (a). The increase in the length SH decreases the second bandwidth as well as the return loss S_{11}. For SH = 1.6 mm, the magnitude of the return loss, operating frequency and the bandwidths are acceptable. Thus, it is selected as the optimized value. Figure 3 (b) depicts the effect of substrate length (SL) on the S_{11}. It can be claimed from the plot that the value of SL highly influences the second operating frequency. The increase in SL reduces the operating frequency heavily. For SL = 27 mm, the second operating frequency is near 1.67 GHz, whereas the first operating frequency is very close to the MICS band. So, it is selected as the optimized value.

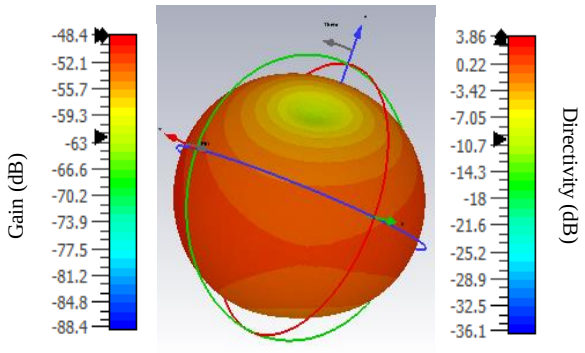

(a)

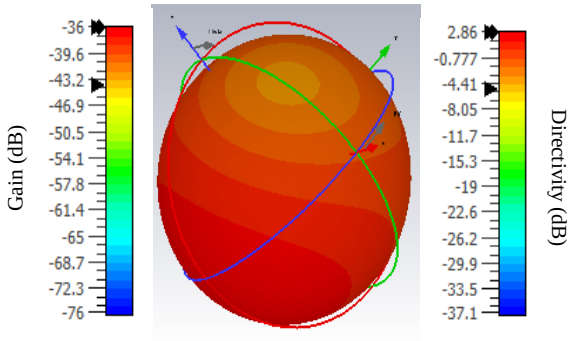

(b)

Figure 4. Gain and directivity for SH = 1.2 mm at (a) 467 MHz, and (b) 1.69 GHz.

Table 2. Gain, directivity and efficiency for different parameters.

Parameter	Value (mm)	Gain (dB)	Directivity (dB)	Efficiency (dB)
SH	1.2	-48.4 -36.0	3.86 2.86	-12.53 -12.58
	1.4	-47.3 -25.0	4.52 3.10	-10.46 -8.06
	1.6	**-45.7** **-18.2**	**5.74** **3.90**	**-7.96** **-4.67**
SL	31	-45.4 -35.0	4.85 3.86	-9.36 -9.06
	29	-44.3 -25.0	5.51 3.10	-8.03 -8.06
	27	**-45.2** **-18.8**	**6.74** **4.90**	**-6.70** **-3.83**
W1	1.4	-51.4 -40.1	3.29 1.47	-15.62 -27.27
	1.5	**-45.3** **-18.4**	**5.01** **2.82**	**-9.06** **-6.52**
	1.7	-48.9 -28.2	4.56 1.94	-10.72 -14.53
W	1.4	-42.4 -30.1	4.27 2.47	-9.92 -12.18
	1.2	**-45.5** **-18.8**	**5.79** **2.89**	**-7.85** **-21.12**
	1.0	-49.9 -23.2	3.50 1.92	-14.25 -12.08

Figure 3 (c) illustrates the simulated S_{11} with several values of the width of the spiral arm (W1). It does not affect the operating frequencies much, but it severely affects the magnitude of the return loss.

For W1 = 1.6 mm, the magnitude of the return loss, the operating frequency, and the bandwidths are acceptable. So, it is selected as the optimized value. The effect of the width of the patch slots (W) is shown in Figure 3 (d). It does not affect the operating frequencies much, but it severely affects the magnitude of the return losses at both frequencies. The best performance is obtained for W = 1.2 mm.

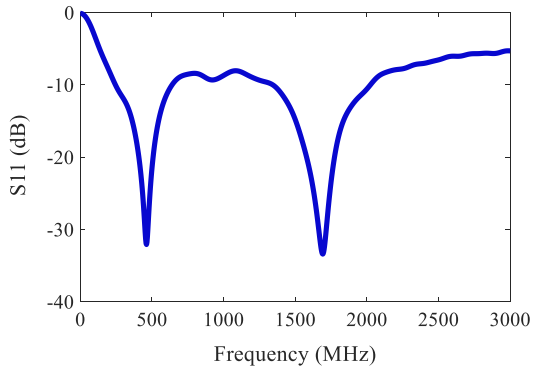

Figure 5. Return loss S_{11} of the proposed antenna.

After the analysis, it can be said that the optimized set of values for the parameters are SH = 1.6 mm, SL = 27 mm, W1 = 1.5 mm, and W = 1.2 mm.

In Figure 4, the radiation pattern for SH = 1.2 mm is depicted, illustrating the values of gain and directivity in decibels. Similarly, the radiation pattern for various values of SH and other parameters (SL, W1 and W) are observed. The resulting gain and directivity values are detailed in Table 2. Efficiency values are computed by dividing the gain by the respective directivity values.

According to the results shown in Table 2, it is seen that the maximum efficiency is obtained for SH = 1.6 mm, SL = 27 mm, W1 = 1.5 mm, and W = 1.2 mm. Hence, this set parameters is selected as the optimized parameters.

3. Results and Discussion

3.1. Return Loss (S_{11} Parameter)

Figure 5 illustrates the variation of the return loss S_{11} of the proposed antenna for the optimized set of parameters. According to the simulated results, the return losses for the resonance frequencies of 459 MHz and 1.68 GHz are -31.98 dB and -33.16 dB, respectively, referring to very small power loss due to reflection.

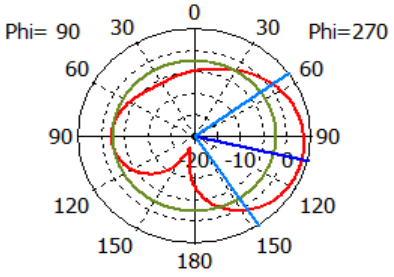

(a)

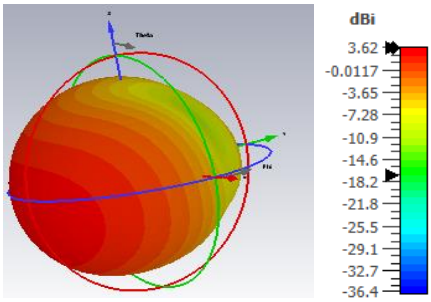

(b)

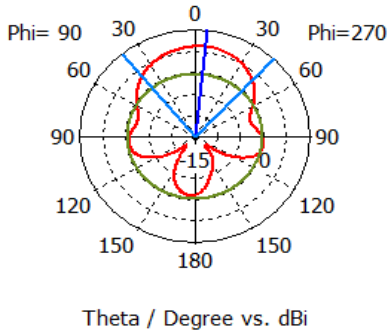

(c)

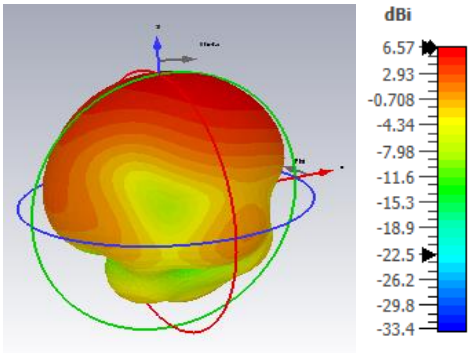

(d)

Figure 6. Radiation pattern of the antenna at 459 MHz in (a) 1D form and (b) 3D form and at 1.68 GHz in (c) 1D form and (d) 3D form.

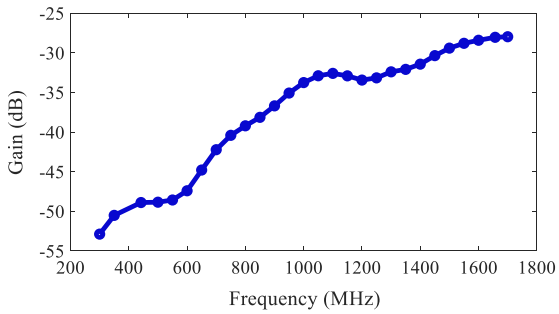

Figure 7. Realized gain of the proposed antenna.

While the second operating frequency is in the L band, the first operates close to the MICS band.

3.2 Radiation Pattern

Figure 6 depicts the radiation pattern of the proposed antenna obtained from simulation. According to the results, the main lobe magnitudes at resonance frequencies of 459 MHz and 1.68 GHz are 2.22 dB and 5.75 dB, respectively, with directions along -70 degrees and 3 degrees. It is observed that the beam direction at different frequency bands is not the same. Because each resonant frequency excites a distinct current distribution

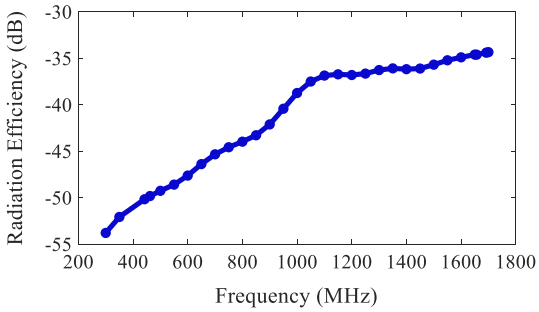

Figure 8. Radiation efficiency of the proposed antenna.

on the patches. This shift in current distribution directly affects the radiating element's effective phase center, altering the beam direction [18].

3.3 Gain

The obtained gain of the proposed antenna is illustrated in Figure 7. The maximum gains at resonance frequencies of 459 MHz and 1.68 GHz are - 45.6 dB and - 18.2 dB, respectively, which signifies the ability of the antenna to amplify the signal power compared to an isotropic antenna at corresponding frequencies.

3.4 Efficiency

The variation in radiation efficiency with respect to the frequency of the proposed antenna is shown in Figure 8. At 459 MHz and 1.68 GHz, respectively, the radiation efficiencies are - 49.18 dB and - 20.99 dB. They quantify the percentage of input power delivered to the antenna that gets radiated as electromagnetic waves. A higher radiation efficiency implies less power loss within the antenna structure, leading to stronger radiated signals.

Due to the lack of laboratory facilities e.g., unavailability of network analyzer and anechoic chamber, the experimental results could not be obtained to validate the antenna performance. In the absence of experimental data, we emphasize that our simulation methodology utilizes validated computational tool (CST). The simulation setup incorporates realistic material properties, environmental conditions, and operational parameters to accurately model the behaviour of the antenna. Furthermore, our simulation results are consistent with theoretical predictions and prior empirical studies available in the literature.

4. Comparison with the Existing Models

This paper introduces a novel spiral patch antenna design augmented with patch slots and a shortening pin, resulting in enhanced return loss characteristics and increased bandwidth. Previous studies have explored diverse methodologies, including unslotted spiral

patches, fractal structures, cubic configurations, and DGS, each offering distinct advantages. A comparative analysis of the proposed antenna geometry with the antennas reported in previous studies is presented in Table 3.

According to comparative analysis shown in Table 3, the proposed antenna provides higher bandwidths compared to other antennas with sufficient gain. Though the antenna proposed in [19] has higher bandwidths, the proposed antenna exhibits a more compact form factor. Furthermore, the present design integrates both patch slots and a shortening pin alongside coaxial feeding within the spiral patch, a configuration not utilized in the previous studies. This combination contributes to enhanced impedance matching, resulting in reduced return losses. Additionally, the proposed design has a relatively simple structure compared to alternative antenna configurations.

5. Conclusion

A two-port coaxial probe fed spiral shaped dual-band antenna for wireless communication is introduced in this work. The proposed antenna is designed to operate at two different frequencies: 459 MHz, which is close to the MICS band, and 1.68 GHz, in the L band. It offers bandwidths of 416 MHz and 800 MHz for each resonant frequency, respectively. The antenna is made on an FR-4 substrate and consists of two symmetrical spiral elements, measuring 27 × 14 × 1.6 mm^3 in total. The coaxial probe feeding technique is used for excitation. This antenna demonstrates low power loss because of the improved return losses, which are - 31.98 dB and - 33.16 dB at their respective resonant frequencies. Patch slots and shortening pins are incorporated in the spiral patches to improve their return loss and increase bandwidths, representing a significant contribution to the field of dual-band antenna design for wireless communication. Given the capability of the proposed antenna to operate within both the MICS band and L band, it possesses the versatility to be employed for applications in biomedical contexts, as well as in mobile or satellite communications. At the resonant frequencies, gains of - 45.6 dB and - 18.2 dB are finally realized with radiation efficiencies of -49.18 dB and - 20.99 dB, respectively. Due to the limitations of resources and lab facilities, the proposed antenna could not be fabricated. Thus, the experimental results could not be obtained.

Table 3. Comparative analysis of the proposed antenna model with the existing antenna models.

Ref	Size (mm^3)	Antenna Type	Resonant Frequency (MHz)	Bandwidth (MHz)	Gain (dB)
[19]	17.92	Cavity Slot	2450	670	-26.5
[20]	28.85	Spiral Patch	915	915	-28
[21]	57.3	Fractal	403 2440	92 320	-28.1 -31.3
[22]	3375	Cubic	2450 5800	900 1500	-18.5
[23]	15.87	Patch	1400 2450	300 380	-27.6 -27.1
[24]	367	Helical	2450	-	-32
[25]	139.7	Slot	402	-	-27.7
[26]	24	Meander Patch	915 2450	-	-28.5 -22.8
Proposed Design	480	Spiral Patch with Slots	459 1680	416 800	-45.6 -18.2

References

[1] A. G. Miquel, “Antenna design and characterization for biomedical applications,” University of Barcelona, Barcelona, Spain, Oct. 2018.

[2] A. Zakaria et al., “Design and Modeling of Ultra-Compact Wideband Implantable Antenna for Wireless ISM Band,” Bioengineering, vol. 10, no. 2, pp. 216–216, Feb. 2023.

[3] A. M. Mozi, D. S. A. Damit, and Z. Faiza, “Rectangular spiral microstrip antenna for WLAN application,” IEEE Control and System Graduate Research Colloquium (ICSGRC), Selangor, Malaysia, Jul. 2012.

[4] S. K. Padhi, N. C. Karmakar, C. L. Law, and S. Aditya, “A dual polarized aperture coupled circular patch antenna using a c-shaped coupling slot,” IEEE Transactions on Antennas and Propagation, vol. 51, no. 12, pp. 3295–3298, Dec. 2003.

[5] W.-C. Liu, C. Wu, and Y. Dai, “Design of Triple-Frequency Microstrip-Fed Monopole Antenna Using Defected Ground Structure,” IEEE Transactions on Antennas and Propagation, vol. 59, no. 7, pp. 2457–2463, May 2011.

[6] A. Arif, M. Zubair, M. Ali, M. U. Khan, and M. Q. Mehmood, “A Compact, Low-Profile Fractal Antenna for Wearable On-Body WBAN Applications,” IEEE Antennas and Wireless Propagation Letters, vol. 18, no. 5, pp. 981–985, May 2019.

[7] Z. Duan, Y.-X. Guo, R.-F. Xue, M. Je, and D.-L. Kwong, “Differentially Fed Dual-Band Implantable Antenna for Biomedical Applications,” IEEE Transactions on Antennas and Propagation, vol. 60, no. 12, pp. 5587–5595, Dec. 2012.

[8] P. Soontornpipit, C. M. Furse, and Y. C. Chung, “Design of Implantable Microstrip Antenna for Communication

with Medical Implants," IEEE Transactions on Microwave Theory and Techniques, vol. 52, no. 8, pp. 1944–1951, Aug. 2004.

[9] Md. S. Islam, K. P. Esselle, D. Bull, and P. M. Pilowsky, "Converting a Wireless Biotelemetry System to an Implantable System Through Antenna Redesign," IEEE Transactions on Microwave Theory and Techniques, vol. 62, no. 9, pp. 1890–1897, Sep. 2014.

[10] F.-J. Huang, C.-M. Lee, C.-L. Chang, L.-K. Chen, T.-C. Yo, and C.-H. Luo, "Rectenna Application of Miniaturized Implantable Antenna Design for Triple-Band Biotelemetry Communication," IEEE Transactions on Antennas and Propagation, vol. 59, no. 7, pp. 2646–2653, Jul. 2011.

[11] V. Kaim, B. K. Kanaujia, S. Kumar, H. C. Choi, K. W. Kim, and K. Rambabu, "Ultra-Miniature Circularly Polarized CPW-Fed Implantable Antenna Design and its Validation for Biotelemetry Applications," Scientific Reports, vol. 10, no. 1, Apr. 2020.

[12] Z. A. Dayo et al., "A novel compact broadband and radiation efficient antenna design for medical IoT healthcare system," Mathematical Biosciences and Engineering, vol. 19, no. 4, pp. 3909–3927, 2022.

[13] A. Y. I. Ashyap et al., "Robust and Efficient Integrated Antenna With EBG-DGS Enabled Wide Bandwidth for Wearable Medical Device Applications," IEEE Access, vol. 8, pp. 56346-56358, 2020.

[14] A. Zakaria et al., "Design and Modeling of Ultra-Compact Wideband Implantable Antenna for Wireless ISM Band," Bioengineering, vol. 10, no. 2, pp. 216–216, Feb. 2023.

[15] Z. Huang, H. Wu, S. S. Mahmoud, and Q. Fang, "Design of a Novel Compact MICS Band PIFA Antenna for Implantable Biotelemetry Applications," Sensors, vol. 22, no. 21, p. 8182, Oct. 2022.

[16] M. Palandoken, "Compact Bioimplantable MICS and ISM Band Antenna Design for Wireless Biotelemetry Applications," Radioengineering, vol. 26, no. 4, pp. 917–923, Dec. 2017.

[17] Y. Fan, H. Liu, X. Liu, Y. Chen, Z. Li, and M. M. Tentzeris, "Novel coated differentially fed dual-band fractal antenna for implantable medical devices," IET Microwaves Antennas & Propagation, vol. 14, pp. 199–208, 2019.

[18] V. R. Gudivada et al., "Dual-Band Pattern Diversity Liquid Antenna with Passive Beam-Steering of the Broadside Modes," IET Microwaves, Antennas & Propagation, 2024.

[19] W. Xia, K. Saito, M. Takahashi, and K. Ito, "Performances of an Implanted Cavity Slot Antenna Embedded in the Human Arm," IEEE Transactions on Antennas and Propagation, vol. 57, no. 4, pp. 894–899, Apr. 2009.

[20] A. Basir and H. Yoo, "A Stable Impedance-Matched Ultrawideband Antenna System Mitigating Detuning Effects for Multiple Biotelemetric Applications," IEEE Transactions on Antennas and Propagation, vol. 67, no. 5, pp. 3416–3421, May 2019.

[21] Y. Fan, H. Liu, X. Liu, Y. Chen, Z. Li, and M. M. Tentzeris, "Novel coated differentially fed dual-band fractal antenna for implantable medical devices," IET Microwaves Antennas & Propagation, vol. 14, no. 2, pp. 199–208, Nov. 2019.

[22] V. Kaim, B. K. Kanaujia, and K. Rambabu, "Quadrilateral Spatial Diversity Circularly Polarized MIMO Cubic Implantable Antenna System for Biotelemetry," IEEE Transactions on Antennas and Propagation, vol. 69, no. 3, pp. 1260–1272, Mar. 2021.

[23] J. Zhang et al., "A Compact Dual-Band Implantable Antenna for Wireless Biotelemetry in Arteriovenous Grafts," IEEE Transactions on Antennas and Propagation, vol. 71, no. 6, pp. 4759–4771, Jun. 2023.

[24] C. Liu, Y.-X. Guo, and S. Xiao, "Circularly Polarized Helical Antenna for ISM-Band Ingestible Capsule Endoscope Systems," IEEE Transactions on Antennas and Propagation, vol. 62, no. 12, pp. 6027–6039, Dec. 2014.

[25] H. Li, Y.-X. Guo, C. Liu, S. Xiao, and L. Li, "A Miniature-Implantable Antenna for MedRadio-Band Biomedical Telemetry," IEEE Antennas and Wireless Propagation Letters, vol. 14, pp. 1176–1179, 2015.

[26] S. A. A. Shah and H. Yoo, "Scalp-Implantable Antenna Systems for Intracranial Pressure Monitoring," IEEE Transactions on Antennas and Propagation, vol. 66, no. 4, pp. 2170–2173, Apr. 2018.